NUCL SCI TECH (2019) 30:98
https://doi.org/10.1007/s41365-019-0618-y

Determining the effect of relative size of sensor on calibration accuracy of TEM cells

Yun-Sheng Jiang[1,2] · Cui Meng[1,2] · Han-Bing Jin[1,2] · Ping Wu[1,2] · Zhi-Qian Xu[1,2] · Liu-Hong Huang[1,2]

Received: 26 September 2018 / Revised: 26 February 2019 / Accepted: 1 March 2019 / Published online: 18 May 2019

Abstract The time-domain calibration coefficient of a D-Dot sensor should be identical across various transverse electromagnetic (TEM) cells to comply with the IEEE Std 1309. However, in our previous calibration experiments, poor consistency was observed. The size of D-Dot sensors relative to TEM cells is considered the main reason for this poor consistency. Therefore, this study aims at determining the calibration coefficient of a D-Dot sensor. We calculate the theoretical coefficient as a reference. Practical calibration experiments involve the processing of TEM cells with three different sizes. To observe the response more clearly, corresponding models are constructed and numerical simulations are performed. The numerical simulations and experimental calibration are in good agreement. To determine the calibration accuracy, we quantify the accuracy using the relative error of the calibration coefficient. By comparing the coefficients obtained, it can be concluded that the perturbation error is about 15% when the relative size is over 1/3. Further, the relative size should be less than 1/5 to obtain a relative error below 10%.

Keywords D-Dot · Electromagnetic sensor · Time-domain calibration · Accuracy · Numerical simulation

✉ Cui Meng
mengcui@mail.tsinghua.edu.cn

[1] Key Laboratory of Particle and Radiation Imaging, Ministry of Education, Beijing 100084, China

[2] Department of Engineering Physics, Tsinghua University, Beijing 100084, China

1 Introduction

Recently, along with the decreasing features size and increasing degree of integration of electronic devices, such as preamplifiers in readout electronics, the operating frequency has increased [1]. The wide bandwidth and high-power transient electromagnetic (EM) field has significantly increased the threat to electronic systems [2, 3], such as function failure and destruction. Therefore, there is a need for a proper electromagnetic compatibility (EMC) assessment. In related research and assessments, the measurement of the EM fields is a major task.

The use of electric field sensors or probes is the most direct approach to measure transient electric fields. In order to obtain the actual field strength from the sensor measurements, calibration is required prior to operation. Compared to the ANSI C63.5-1998, the IEEE Std 1309-1996 standard provides a more targeted method for transient electric field calibration [4]. The calibration of sensors can be divided into two parts, namely time-domain calibration and frequency-domain calibration. For a sensor that satisfies the frequency criterion, time-domain calibration is the most important step in determining the relationship between the output signal and the actual electric field. Method B in IEEE Std 1309-1996 is a frequently used time-domain calibration method, which produces a quantifiable EM field using specific equipment, such as a transverse electromagnetic (TEM) cells, to obtain the calibration coefficients of the EM field sensor. However, an EM sensor is usually made of metal, which perturbs the electric field. With regard to an EM sensor, the TEM cell is a limited space with metal boundaries. Therefore, there is a field perturbation over the volume of the D-Dot sensor, which causes the calibration inaccuracy.

There are very few published papers that focus specifically on calibration accuracy, but several researchers reported studies involving calibration in TEM cells. In 1974, Crawford made a rather fine design of a TEM cell and discussed the electric field distribution in detail [5]. His approach was subsequently adopted in accuracy control estimation before calibration [6]. In 1999, Garn et al. [7] limited the upper frequency of calibration to 500 MHz and analyzed the frequency characteristics of precision reference dipole (PRD) antennas using a TEM cell. The conclusions were incorporated into the IEEE Std 1309. Cui et al. [8] also proved that different kinds of pulse waveforms provide sensor calibration with good consistency. Toshio Morioka investigated the response to a non-uniform E-field strength [9]. Jeon et al. [10] also verified TEM modes with statistical methods. Wang et al. [11] reported a compensation method to remove the coupling effect of isotropic calibration.

For time-domain calibration, the IEEE Std 1309-1996 and the latest version [12] limit the probe size relative to parameters such as the plate separation, dynamic range and maximum interception alignment. For the calibration of EM sensors in TEM cells, IEC 61000-4-20 also provides some informative limits. In most cases, the requirement is the same. However, there is a slight discrepancy between these two standards on the relative probe size. In our previous calibration experiments, we observed that, in accordance with IEEE Std 1309, the calibration coefficients for the same D-Dot sensor are 3.757 and 4.789 in the 300- and 400 MHz TEM cells, respectively, which shows poor consistency. In subsequent research, the effects of the sensor size relative to the TEM cell were considered. Therefore, this study investigates the calibration error of a sensor with different TEM cells, with the aim of increasing the calibration accuracy of a transient electric field sensor.

Among the various electromagnetic field sensors, the D-Dot sensor is the most suitable for research on the calibration accuracy. Because all parts of a D-Dot sensor can be designed, machined and assembled precisely, the theoretical calibration coefficients can be easily calculated. Therefore, in this study we adopt the D-Dot sensor to represent electric field sensors.

This paper starts from a description of the D-Dot sensor and the setup for the calibration. The theoretical calibration coefficient is calculated, and the setup for the calibration used for the IEEE Std 1309 values is presented. Then, we describe the numerical simulation and the practical experiments, along with the calibration coefficients that were obtained. We then analyze the calibration accuracy and summarize the paper. Finally, some suggestions are proposed.

2 D-Dot sensor and calibration setup

2.1 Transient field sensor D-Dot

There are many types of transient electric field sensors or probes, including the E-field sensor, EM-Dot sensor, electro-optic electric field sensor and D-Dot sensor [13–17]. The D-Dot sensors are the most commonly used and have unique advantages, such as simple structure, tiny volume and rapid response during the measurement of the electric field in pulsed power equipment [18].

The D-Dot sensor is constructed using mainly two metal heads connected to a fixed load. The equivalent electric circuit is shown in Fig. 1. Owing to the fine design and structure, when there are specific parameters, the theoretical calibration coefficient of the two heads can be easily calculated, which may be a reference standard for other calibration methods. However, the practical calibration process is still necessary for each experimental setup. Moreover, because some sensors' calibration relationships are difficult to obtain theoretically, it is important to investigate the calibration accuracy.

A balun is a type of balanced–unbalanced transformer, used to transform the balanced signal into an unbalanced signal, or vice versa [19]. It can eliminate the common-mode current and help to match the impedance between two connected devices. A Montena BL 3–5 G balun with a characteristic impedance of 50 Ω was used [20]. To achieve impedance matching, the impedance of the D-Dot sensor (Z_c) was also set to 50 Ω.

The metal head of the D-Dot sensor has a "teardrop" shape. The shape near the feed point is a cone. The pulse impedance of the conical antenna can be designed from the following equation [21]:

$$Z_C = \frac{1}{2\pi}\sqrt{\frac{\mu_0}{\varepsilon_0}}\ln\left(\cot\left(\frac{\theta}{2}\right)\right), \tag{1}$$

where ε_0 is the vacuum dielectric constant, μ_0 is the permeability of vacuum and θ represents the half-cone angle of the D-Dot sensor. Clearly, by setting Z_c to 50 Ω, a half-cone angle of $\theta = 46.96°$ is obtained.

The shape and height of the metal head were calculated in accordance with the equivalent charge method [22].

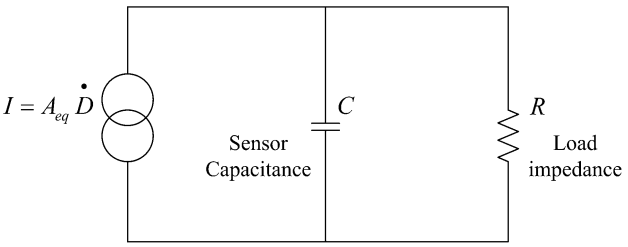

Fig. 1 Schematic of a D-Dot sensor's equivalent circuit

Then, the calibration coefficients and frequency band were calculated accordingly.

We now describe the calibration coefficients calculations. The output voltage drop on the load was recorded using an oscilloscope. Let f represent the maximum frequency of the sensor and let C represent the capacitance of the electric circuit. Considering that $2\pi f < 1/RC$, the relationship between the output voltage V_L and incident electric field E is [23]:

$$V_L(t) = R \cdot A_{eq} \cdot \varepsilon_0 \cdot \frac{\partial}{\partial t} E(t). \tag{2}$$

By integrating Eq. (2), the equation becomes:

$$E(t) = K \cdot Y(t) = K \cdot \int V_L(t)\mathrm{d}t = \frac{1}{R \cdot A_{eq} \cdot \varepsilon_0} \int V_L(t)\mathrm{d}t, \tag{3}$$

where R represents the resistance of the balun and K is the calibration coefficient of the sensor. A_{eq} is the equivalent area of the D-Dot sensor and can be calculated depending on the shape of the metal head, as follows [24]:

$$A_{eq} = -\frac{h^2\pi\left[1 - \left(\tan\frac{\theta}{2}\right)^2\right]}{\ln\left(\tan\frac{\theta}{2}\right)}, \tag{4}$$

where h represents the height of the head. The coefficient can be calculated according to the parameters introduced above.

The frequency band can be determined by the following procedure. The frequency band is restricted by an upper and a lower frequency. The upper frequency is mainly limited by the time constant of the sensor and is determined by the following equation:

$$f_t = \frac{1}{2\pi RC}. \tag{5}$$

By performing complex calculations, the capacitance of the D-Dot sensor can be derived as [22]:

$$C = -\varepsilon_0 \pi h \frac{1 - \left(\tan\frac{\theta}{2}\right)^2}{\ln\left(\tan\frac{\theta}{2}\right)}. \tag{6}$$

And the lower frequency is:

$$f'_\infty = -\frac{1}{4}\frac{1 - \left(\tan\frac{\theta}{2}\right)^2}{\ln\left(\tan\frac{\theta}{2}\right)}. \tag{7}$$

Therefore, the frequency can be limited within $f_\infty{}'$ and f_t. The calculated frequency band of the D-Dot sensor ranges from 0.233 Hz to 8.18 GHz.

The parameters of the D-Dot sensor designed by the laboratory of the Tsinghua University Electromagnetic Pulse Environment and Effect are the following: The half-cone angle θ is 46.96°, and the height of the metal head is 15 mm [24]. A photograph of the D-Dot sensor is shown in Fig. 2. The circular plate between the metal heads, which has radius of 30 mm, is used to minimize the effects of the assembly error, asymmetry of metal heads, etc.

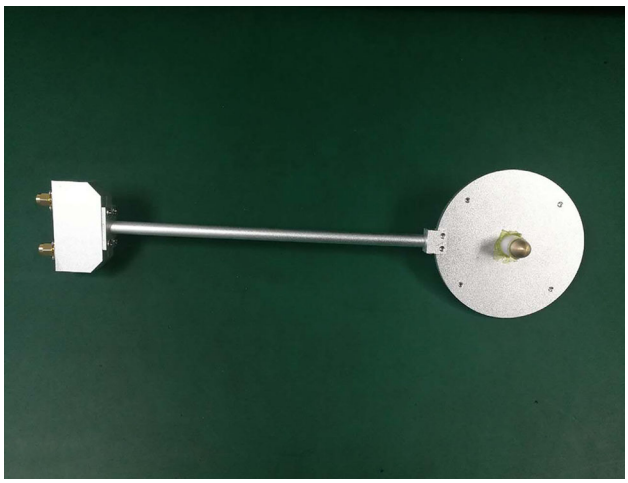

Fig. 2 D-Dot sensor

Therefore, the equivalent area can be calculated as: $A_{eq} = 6.8779 \times 10^{-4}\,\mathrm{m}^3$, and the theoretical calibration coefficient is $K_{the} = 3.286 \times 10^{12}\,\mathrm{m}^{-1}\,\mathrm{s}^{-1}$.

2.2 TEM cell

The TEM cell is a standard calibration equipment described in IEEE Std 1309. It is also known as a closed TEM waveguide in IEC 61000-4-20. It generates a quantifiable and known uniform electric field, which can be used to test the response of an EM field sensor or probe. In addition, TEM cells are also used in EMC tests for emission and susceptibility testing [25, 26]. The operation of a TEM cell is also described in IEC 61000-4-20.

A TEM cell is a modified coaxial transmission cable. Its structure is simple and includes an outer shield and an inner septum. The main function of TEM cells is to produce a uniform field. For ideal parallel plates, the calculation of an electric field is as follows:

$$E_v = \frac{\sqrt{P_n R_C}}{b}, \tag{8}$$

where P_n represents the net power input into the TEM cells, R_c represents the impedance of the TEM cell and b represents the distance between the septum and the outer wall. If the reflection or voltage standing wave ratio (VSWR) of the TEM cell is negligible, the equation can be rewritten as:

$$E_v = \frac{V}{b}, \tag{9}$$

where V represents the output voltage of the pulse generator.

For RF testing, the bandwidth is also a significant parameter. For transient tests, the initial frequency is required to be 100 kHz [26] and the upper frequency is related to the size of the TEM cell:

$$f_c = \frac{c}{2a}, \tag{10}$$

where a represents the width of the TEM cell and c represents the speed of light.

Once the size of the TEM cell is specified, the bandwidth is determined. In this paper, a TEM cell with a frequency range of 100 kHz to 300 MHz is called a 300 MHz TEM cell.

The 300 MHz TEM cell is designed and manufactured at the laboratory of the Tsinghua University Electromagnetic Pulse Environment and Effect. The distance between the septum and the outer wall is 0.25 m. Photographs of the 300 MHz TEM cell and the 400 MHz TEM cell, purchased from ETS Lindgren, are shown in Fig. 3. The 100 MHz TEM cell is obtained from the National Institute of Metrology (NIM) of China. The main parameters are listed in Table 1. It is noted that the maximum dimension of the D-Dot sensor is 60 mm, as stated in Sect. 2.1.

The TEM cells exhibit outstanding performances on the input port voltage reflection coefficient (S_{11}) and uniformity of the electric field. The S_{11} values of the 300 and 400 MHz TEM cell are given in Fig. 4.

In IEEE Std 1309, it is stated that the VSWR in TEM cells should generally be less than 1.5:1, to ensure that frequencies are below the higher-order mode cutoff. In accordance with the VSWR value, the S_{11} should be less than − 14 dB. Therefore, a baseline of − 14 dB is set for the frequency band criteria, and the frequency band is considered to be suitable in the calibration for which the values are below the baseline. Figure 4 shows that the upper frequency of the 400 MHz TEM cell can exceed 500 MHz and the upper frequency of the 300 MHz TEM cell can reach approximately 350 MHz. According to the NIM, the upper frequency of the 100 MHz TEM cell can exceed 120 MHz.

Fig. 3 **a** Schematic of the 300 MHz TEM cell, **b** schematic of the 400 MHz TEM cell

2.3 Standard setup of calibration system

According to method B described in the IEEE Std 1309-1996, the schematic of the instrument setup of a transient electric field sensor is as shown in Fig. 5.

In this paper, the TEM cell is used as an "electromagnetic simulator" and the D-Dot sensor is used as a "field sensor under test."

The detailed setup is described as follows. A pulse generator is connected to one port of TEM cell to excite a pulsed EM field. The D-Dot sensor that is to be calibrated, joint with a balun, is placed inside the TEM cell. We aligned the center of the D-Dot sensor's head with the center of the TEM cell. Furthermore, we aligned the D-Dot sensor to achieve the maximum reception of the applied field vector, which is perpendicular to the septum of the TEM cell. The output signal of the balun is directly connected to an oscilloscope. At the same time, the signal output from the TEM cell is recorded with the same oscilloscope via an attenuator. After the acquisition, data processing is required to obtain the calibration coefficient.

3 Influence of relative size

In our previous study, it was found that the insertion of a sensor into a TEM cell can clearly perturb the EM field [27]. Further, the relative rate of change of the electric field strength on the highest point of the metal head is particularly high and can reach an order of 10 [27]. Because of the finite frequency bandwidth, the effect of the high-frequency perturbation is hardly reflected in the response of a sensor. We define the relative size of the D-Dot sensor as the ratio of the maximum dimension of the sensor to the distance between the septum and the outer wall of the TEM cell. The relative error δ_K is defined in (11), which represents the quantitative influence of the relative size.

$$\delta_K = \frac{K - K_{the}}{K_{the}}, \tag{11}$$

where K represents the electric field obtained in the experiments or the calculations. K_{the} represents the theoretical value calculated in part 2.1.

3.1 Practical calibration experiments

The equipment is connected as shown in Fig. 5. In this study, an FCC pulse generator was used to generate a dynamic output voltage in the range of 0–2.0 kV. A Tektronix DPO 5205B oscilloscope was used to record the measurement signal of the sensor. For impedance matching, the port impedance of the oscilloscope was set to 50 Ω.

Table 1 Main parameters of TEM cells

Calibration equipment name	Cutoff frequency (MHz)	Distance between septum and outer conductor (b)	Ratio of maximum dimension of D-Dot sensor and TEM cell
100 MHz TEM	100	0.45 m	$< 1/5$
300 MHz TEM	300	0.25 m	$< 1/3$
400 MHz TEM	400	0.15 m	$\sim 1/3$

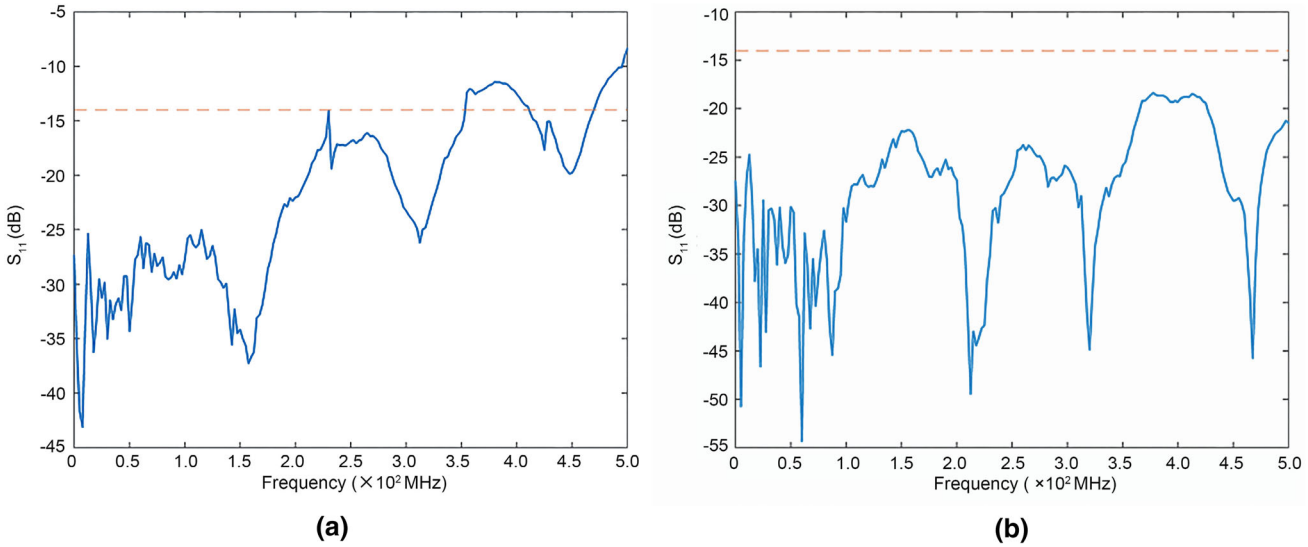

Fig. 4 S_{11} measured with a vector network analyzer, with the frequencies ranging from 9 kHz to 500 MHz. **a** S_{11} of 300 MHz TEM cell, **b** S_{11} of 400 MHz TEM cell

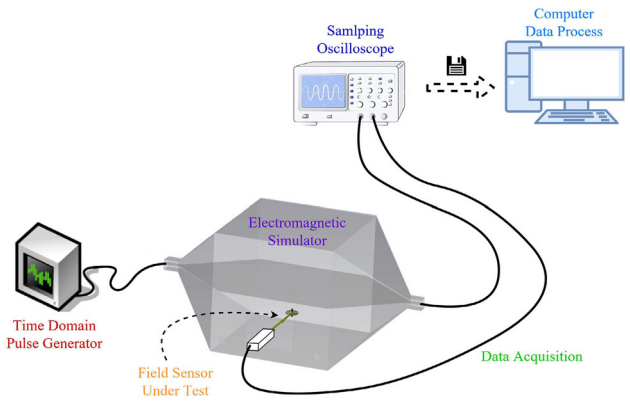

Fig. 5 Schematic of instrument setup

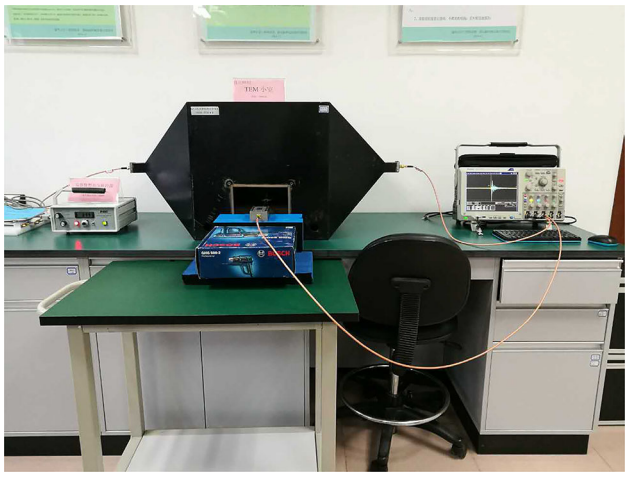

Fig. 6 Experimental setup for the 300 MHz TEM cell calibration

The setup of the calibration experiment in the 300 MHz TEM cell is illustrated in Fig. 6.

Because practical experiments involve issues such as noise and integration and fitting method inaccuracies, the amplitudes of the restored waveform and the excitation signal contain some deviations that are not easily eliminated by averaging the repeated measurements. To stabilize the fitted line, we adopted seven different amplitudes that are suitable in practice. We adjusted seven different amplitudes of the pulse generator to change the electric field strength inside the TEM cell in order to obtain the corresponding output signal.

The setup and procedure are the same for the two TEM cells.

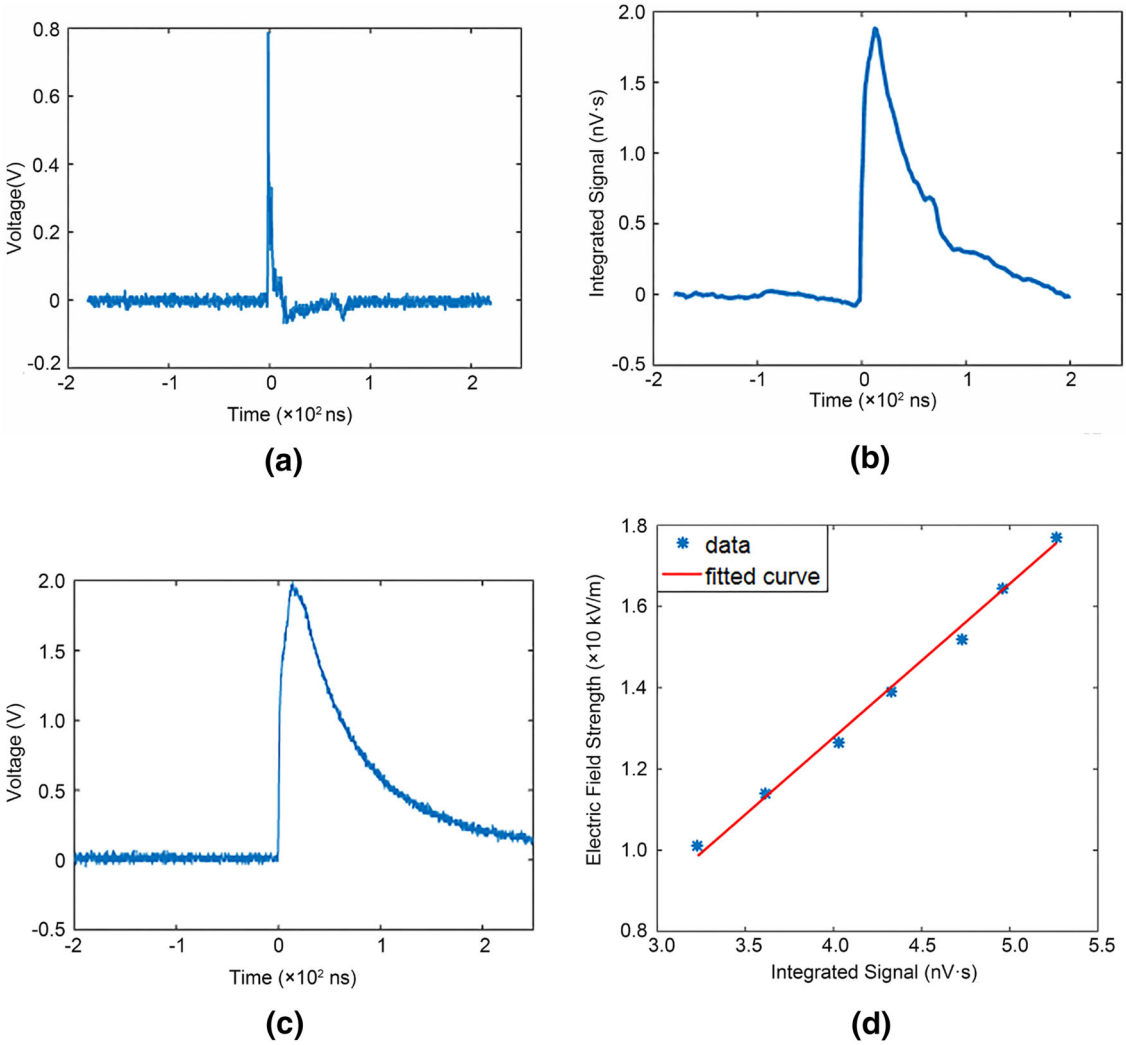

Fig. 7 Procedure of data processing from the 300 MHz TEM cell. **a** Waveform data obtained directly from D-Dot sensor. **b** Integration of **a** with the tilted baseline reduced. **c** Waveform of attenuated excitation signal. **d** Points determined by the amplitudes of the excitation signal and the integrated sensor's data, and a linear fitted line

3.1.1 Experimental results

As previously described, one calibration experiment includes seven different pulse amplitudes. Each amplitude experiment should be repeated seven times to reduce the uncertainty.

Based on Eq. (3), the calibration coefficient should be obtained from the relationship between the electric field $E(t)$ and the integral of the corresponding output voltage $Y(t)$. Because the relationship is always valid for D-Dot sensors, the burst peak measurement is a practical method to obtain the calibration coefficient. For the pulse signals of $E(t)$ and $Y(t)$, the peaks are in correspondence with each other. Therefore, in every experiment, only the amplitudes of $E(t)$ and $Y(t)$ are recorded and adopted to ensure the time correspondence. In order to obtain the linear relationship, several different amplitudes are needed. From the slope of the line, the calibration coefficient K can be easily obtained.

For clarity, we call a "series" of different amplitudes and a "set" of data with the same amplitude. Based on this statement, the data-processing procedure is as shown in Fig. 7:

1. Data acquired from the D-Dot sensor is a time derivative signal of the incident EM field signal, as shown in Fig. 7a;
2. Data from the D-Dot sensor are integrated with trapezoidal integration to resume the original electric field waveform, as shown in Fig. 7b. Then, the amplitude of the resumed waveform is obtained;
3. As illustrated in Fig. 7c, the excitation signal is also recorded with the oscilloscope, and the amplitude of the excitation signal is obtained;

Table 2 Calibration coefficients obtained in the practical experiment

Calibration equipment	Experimental calibration coefficient ($\times 10^{12}\ m^{-1}\ s^{-1}$)	Relative error (δ_K) (%)
100 MHz TEM	3.489	6.2
300 MHz TEM	3.757	14.3
400 MHz TEM	4.789	31.4

4. In each set, there are seven amplitudes of the resumed waveform, and seven corresponding amplitudes of the excitation signal are obtained. In order to reduce the jitter, we average the two classes of amplitudes to obtain two average values.
5. To determine the relationship between the electric field strength and the integrated signal, the electric field generated in the TEM cell should be derived from the amplitude using (9). Then, one set of data can determine a point. The abscissa of the points represents the integrated signal, while the vertical coordinate represents the electric field strength. Therefore, the series of data can identify seven points.
6. As shown in Fig. 7d, the seven points that are obtained in the last step are marked out and linearly fitted. The calibration coefficient K, which is the slope of the fitted line according to (3), is then obtained.

Following the process, the calibration coefficients in the two TEM cells can be obtained by performing practical experiments, as listed in Table 2. The correlation coefficients of the linear fitting are 99.03% in the 100 MHz TEM experiment, 99.49% in the 300 MHz TEM experiment and 99.99% in the 400 MHz TEM experiment.

3.1.2 *Uncertainty analysis*

In the calibration experiments, there are many sources of uncertainty, such as type-A uncertainty, which results from

Table 3 Uncertainty analysis of calibration

Instrument input quality	Basis	Distribution	Uncertainty in X-MHz TEM (dB)		
			100	300	400
Oscilloscope	Type-A	Normal	0.03103		
	Repeated experiments $n = 7$, $\sigma = 0.0821$ dB (equipment specification)	$k = \sqrt{n}$			
Distance of septum and wall (b)/walls of TEM cell	Type-B	Rectangular	0.0334	0.0603	0.1006
	Measurement	$k = \sqrt{3}$			
	Tolerance = 0.0193 dB@100 MHz				
	Tolerance = 0.0348 dB@300 MHz				
	Tolerance = 0.0581 dB@400 MHz				
TEM cell field uniformity	Type-B	Rectangular	0.0059	0.0117	0.0233
	Calculated dimensional effects,	$k = \sqrt{3}$			
	Tolerance = 0.0103 dB@100 MHz				
	Tolerance = 0.0202 dB@300 MHz				
	Tolerance = 0.0405 dB@400 MHz				
Position of sensor	Type-B	Rectangular	0.0222	0.0400	0.0664
	Possible field variation,	$k = \sqrt{3}$			
	Tolerance = 0.0384 dB@100 MHz				
	Tolerance = 0.0692 dB@300 MHz				
	Tolerance = 0.1150 dB@400 MHz				
Feed-in port of TEM cell reflection	Type-B	Rectangular	0.0559	0.0413	0.0156
	Measured refection,	$k = \sqrt{3}$			
	Tolerance = 0.0969 dB@100 MHz				
	Tolerance = 0.0715 dB@300 MHz				
	Tolerance = 0.0270 dB@400 MHz				
Combined standard uncertainty	Rule of propagation of uncertainties (RSS)	Normal	0.0757	0.0897	0.1276
Expanded uncertainty	$k_p \approx 2.10$	Normal	0.16 dB	0.19 dB	0.27 dB

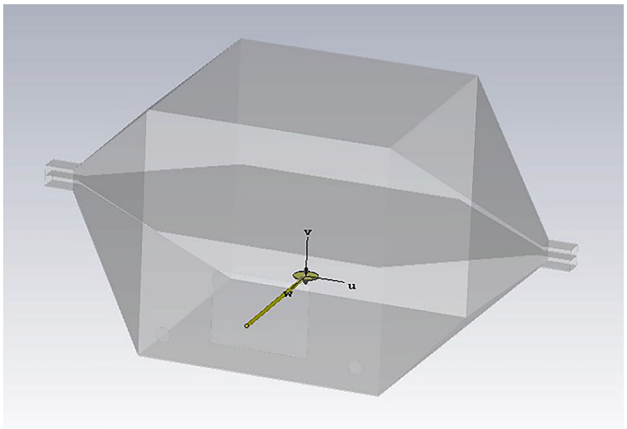

Fig. 8 Model of a 300 MHz-TEM cell with D-Dot sensor

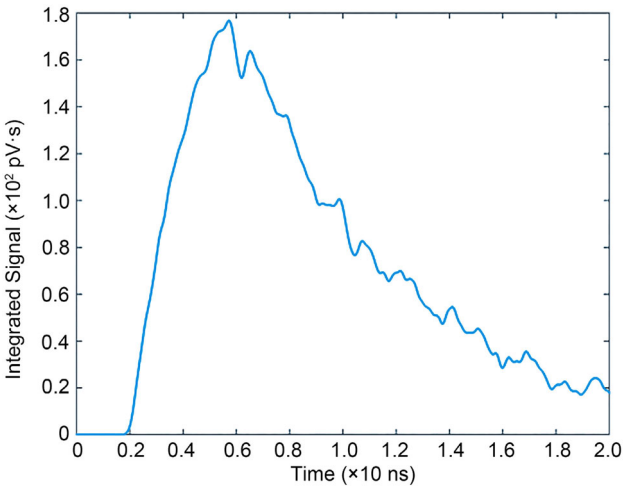

Fig. 9 Waveform measured in the 300 MHz-TEM cell

Table 4 Simulated calibration coefficients K in different equipments

Calibration equipment	Numerical calibration coefficient ($\times 10^{12}$ m^{-1} s^{-1})	Relative error (δ_K)
100 MHz TEM	3.4890	6.2%
300 MHz TEM	3.7875	15.3%
400 MHz TEM	4.2516	29.5%

measurement error of the oscilloscope, and type-B uncertainty, which results from the TEM cell field uniformity, excitation reflection, the position of the sensors, etc. [28]. The uncertainty of the sensor position under the current experimental conditions can be controlled within 2 mm.

With respect to the informative annex E of IEEE Std 1309-2013, which corresponds to ISO/IEC GUIDE 98-3-2008, the uncertainty is directly related to the number of readings n, and the cover factor k_p is indirectly related to n. Empirically, each amplitude experiment was repeated seven times to obtain the average signal amplitude. In this case, the cover factor is k_p= 2.10, which is sufficiently low compared to k_p = 2.00, which is equivalent to the case where n tends to infinity.

A detailed analysis is presented in Table 3.

Therefore, the expanded uncertainties of the calibration are U = 0.19 dB in the 300 MHz TEM cell, U = 0.27 dB in the 400 MHz TEM cell and U = 0.16 dB in the 100 MHz TEM cell, with a coverage factor k_p = 2.10, and a level of confidence of 95%.

3.2 Numerical simulation of calibration

CST MICROWAVE STUDIO® (CST® MWS®) is a specialized tool that is used for three-dimensional (3D) EM simulations of high-frequency components developed by CST. The software provides complete technology on high-frequency, time-domain and 3D EM problems [29]. Using CST MWS, the D-Dot sensor calibration setup and procedure are simulated intuitively to obtain the calibration coefficients.

Three TEM models with different upper useful frequency values and one D-Dot sensor model were constructed using the CST software. The 300 MHz TEM cell, 400 MHz TEM cell and the D-Dot sensor were modeled according to experimental conditions previously described, while the 100 MHz TEM cell was modeled using Ref. [30]. The main parameters of these models correspond to those listed in Table 1.

The placement of the D-Dot sensor in the TEM cell is in accordance with the experiments described above. 3D models of the 300 MHz TEM cell, along with the D-Dot sensor specified in Sect. 2.1, are shown in Fig. 8.

We aligned two waveguide ports on the two sides of the TEM cell in order to simulate the EM input and output. A double-exponential signal was adopted as an excitation signal, fed through port 1 (the input port) into the TEM cell. The rise time was 3 ns, and the total length of the excitation signal was 20 ns. By adjusting the signal power in CST, different amplitudes of feed-in signals could be achieved.

We inserted a lump element between the two heads of the D-Dot sensor, with a resistance of 50 Ω. All of the ports were monitored to check the validity of the port setup and the feed-in signal. The signal output from the lump element was monitored to acquire the time-domain response of the D-Dot sensor.

The waveform of the excitation signal was recorded by monitoring the feed-in port. Then, the sensor's output voltage signal was collected through the lump element. Figure 9 shows the waveform measured in the 300 MHz TEM cell, where the average power of the excitation signal was 5 kW. Obviously, the waveform that was measured by

Table 5 Calibration coefficients and relative errors obtained using three methods

Calibration equipment	Distance between septum and outer conductor	Relative size	Frequency band ($S_{11} < -15$ dB)	Calibration coefficient ($\times 10^{12}$ m^{-1} s^{-1})			Relative error (δ_K)	
				Theoretical	Numerical	Experimental	Numerical simulation (%)	Experimental (%)
100 MHz TEM	0.45 m	< 1/5	100 kHz–131 MHz	3.286	3.3696	3.489 (U = 0.16 dB)	2.54	6.2
300 MHz TEM	0.25 m	< 1/3	100 kHz–350 MHz		3.7875	3.757 (U = 0.14 dB)	15.3	14.3
400 MHz TEM	0.15 m	~ 1/3	100 kHz–500 MHz		4.2516	4.789 (U = 0.17 dB)	29.5	31.4

the D-Dot sensor encounters time-domain reflectometry (TDR) problems. The jagged waveform represents the echo that is overlaid on the output signal of the original response. Investigations are being carried out to determine how to reduce the jag; thus, we do not consider the error that results from the echo in this study.

The data-processing procedure is the same as that introduced in Sect. 3.1 for the practical experiments. The linearity of the fitted curves in the three different kinds of TEM cells is excellent, as the correlation coefficients of the linear fitting are all greater than 99.99%. The simulated calibration coefficients K in the three TEM cells are listed in Table 4.

4 Conclusion

The calibration results obtained in this study are presented in Table 5.

From these results, it can be concluded that:

- There is a clear perturbation of the sensor in TEM cells, and it is the dominant source of the calibration error;
- The theoretical calculation is reliable as a reference, because the numerical simulation and experimental calibration are in good agreement;
- As the relative size of sensors decreases, the calibration error also decreases. A common method that is employed to decrease the relative size is to increase the size of the TEM cell. However, it should be noted that the upper frequency, which is determined by the size, restricts the selection of TEM cells;
- The relative error is about 15%, although the relative size is below 1/3, while the relative error is below 10% when the relative size is less than 1/5.

The conclusions listed above are clearly reflected in Table 5. Further, the large error in the calibration coefficients can be explained from the perspective of the relative size.

With respect to the relative size, IEEE Std 1309-1996 presents its requirement in its normative annex B, as follows: "If the probe or sensor being calibrated occupies 1/3 or less of the distance b (from septum to the outer wall of the cell), the field perturbation error will be less than 10% for E-field […]"

However, our research indicates that the restriction of the relative size in the standards is not sufficient. Considering the TDR problem, there may be noise, uncertainty or other problems in the calibration procedure, and it needs to be more restrictive to satisfy the controlled calibration accuracy, e.g., 10%. The results of this work show that the perturbation error cannot be lowered to 10% when the relative size is 1/3. Therefore, the relative size needs to be more restrictive.

The informative annex E of IEC 61000-4-20 states that "the dimensions of the calibration volume […] should be smaller than 20% of the distance between the inner and outer conductors (septum height)" [26]. In accordance with the standard, the results presented in this paper provide evidence to validate the claim. When the relative size is less than 1/5, the relative error can be maintained below 10%.

References

1. D. Yang, Z. Cao, X. Qin et al., Readout electronics of a prototype spectrometer for measuring low-energy ions in solar wind plasma. Nucl. Sci. Tech. **27**, 135 (2016). https://doi.org/10.1007/s41365-016-0136-0
2. Y. Cheng, M. Ding, K. Wu et al., Damage effect of typical electronic device under EMP, in *Proc.* ISEIM, Kyoto, Japan, 2011, pp. 491–494. https://doi.org/10.1109/ISEIM.2011.6826320
3. Y.-M. Fang, X.-Y. Xu, J.-S. Tian et al., Design of a control system with high stability for a streak camera using isolated ADC. Nucl. Sci. Tech. **29**, 22 (2018). https://doi.org/10.1007/s41365-018-0361-9
4. IEEE Standard for Calibration of Electromagnetic Field Sensors and Probes, Excluding Antennas, from 9 kHz to 40 GHz, IEEE Standard 1309, 1996. https://doi.org/10.1109/IEEESTD.1996.81094

5. M.L. Crawford, Generation of standard EM fields using TEM transmission cells. IEEE Trans. Electromagn. Compat. EMC **16**(4), 189–195 (1974). https://doi.org/10.1109/TEMC.1974.303364
6. R. Middlekoop, Time-domain calibration of field sensors for electromagnetic pulse (EMP) measurements. IEEE Trans. Instrum. Meas. **40**(2), 455–459 (1991). https://doi.org/10.1109/CPEM.1990.109984
7. H. Garn, M. Buchmayr, W. Müllner, Precise calibration of electric field sensors for radiated-susceptibility testing. Frequenz **53**(9–10), 189–194 (1999). https://doi.org/10.1515/FREQ.1999.53.9-10.189
8. C. Meng, X. Guo, X. Chen et al., Test research of consistency for amplitude calibration coefficients of pulsed electric field sensor. Nucl. Tech. **30**(1), 73–77 (2007). https://doi.org/10.3321/j.issn:0253-3219.2007.01.017 (**in Chinese**)
9. T. Morioka, Probe response to a non-uniform E-field in a TEM cell, in *Proc. CPEM*, Daejeon, 2010, pp. 327–328. https://doi.org/10.1109/CPEM.2010.5543818
10. S. Jeon, J. Kwon, D. Kim, Study of a four-port TEM cell with the statistical approach for the calibration of EM field probe, in *Proc. IEEE CAMA*, Antibes Juan-les-Pins, 2014, pp. 1–3. https://doi.org/10.1109/CAMA.2014.7003341
11. W. Huan, Z. Chen, Compensation method for the coupling error between the EUT and TEM cell in E-field probe isotropic calibration, *2015 IEEE ISEMC, Dresden*, 2015, pp. 1195–1200. https://doi.org/10.1109/ISEMC.2015.7256339
12. IEEE Standard for calibration of electromagnetic field sensors and probes, excluding antennas, from 9 kHz to 40 GHz, IEEE Standard 1309, 2013. https://doi.org/10.1109/IEEESTD.2013.6673999
13. X. Zhang, C. Meng, Y. Liu, Relationship between the shape of electric field probes and their measuring performances, in *Proc. APEMC*, Beijing, China, 2010, pp. 405–408. https://doi.org/10.1109/APEMC.2010.5475730
14. A. Al Agry, R. A. Schill, S. Garner et al., Electromagnetic dot sensor-calibration, in *Proc. IEEE PPC*, Washington. DC, USA, 2009, pp. 1348–1353. https://doi.org/10.1109/PPC.2009.5386391
15. Y.J. Rao, H. Gnewuch, C.N. Pannell et al., Electro-optic electric field sensor based on periodically poled LiNbO3. Electron. Lett. **35**(7), 596–597 (1999). https://doi.org/10.1049/el:19990374
16. C.E. Baum, E.L. Breen, J.C. Giles et al., Sensors for electromagnetic pulse measurements both inside and away from nuclear source regions. IEEE Trans. Electromagn. Compat. EMC **20**(1), 22–35 (1978). https://doi.org/10.1109/TEMC.1978.303690
17. Q. Cheng, J. Ni, C. Meng et al., Study of measurement techniques for strong pulsed electric field. Electron. Test **9**, 6–11 (2008)
18. B. Wei, Y. Gu, R. Zhou et al., Design, calibration and measurement of D-dot monitor for Yang accelerator water transmission line. High Power Laser Part. Beams **5**, 830–834 (2007)
19. E.G. Fubini, P.J. Sutro, A wide-band transformer from an unbalanced to a balanced line. Proc. IRE **35**(10), 1153–1155 (1947). https://doi.org/10.1109/JRPROC.1947.232923
20. Ultra Broadband 3.5 GHz, Montena, Switzerland. http://www.montena.com/fileadmin/technology_tests/documents/data_sheets/Data_sheet_BL3-5G_balun.pdf
21. C. E. Baum, Tiny fast-pulse B-dot and D-dot sensors in dielectric media, Dep. Elect. Comp. Eng., Univ. New Mexico, Albuquerque, New Mexico, USA, SSN 544, 2009
22. C.E. Baum, An equivalent-charge method for defining geometries of dipole antennas, AFWL, Rep. SSN 72, 1969
23. Electromagnetic compatibility (EMC)—part 4-33: testing and measurement techniques—measurement methods for high-power transient parameters, IEC 61000-4-33, 2005
24. C. Yang, Test technology and application of high power electromagnetic field, M.S. thesis, Tsinghua University (2016)
25. Specification for radio disturbance and immunity measurement apparatus and methods Part 1–4: radio disturbance and immunity measuring apparatus–ancillary equipment–radiated disturbances, CISPR 16-1-4 (2007)
26. Electromagnetic compatibility (EMC)—part 4-20: testing and measurement techniques—emission and immunity testing in transverse electromagnetic (TEM) waveguides, IEC 61000-4-20 (2010)
27. Y. Jiang, C. Yang, C. Meng, Theoretical research on calibration accuracy of high power transient electromagnetic field sensors, in *Proc. IEEE CAMA*, Syracuse, NY, USA, 2016, pp. 1–3. https://doi.org/10.1109/CAMA.2016.7815733
28. Uncertainty of measurement—part 3: guide to the expression of uncertainty in measurement (GUM: 1995), ISO/IEC GUIDE 98-3 (2008)
29. CST Microwave Studio. https://www.cst.com/products/cstmws
30. C. Rostamzadeh, B. Archambeault, S. Connor, FDTD analysis of symmetric TEM cell, in *Proc. EMC*, Chicago, IL, USA, 2005, pp. 525–529. https://doi.org/10.1109/ISEMC.2005.1513571